Power absorption at metal surfaces

J.-T. Lee and W. L. Schaich
Physics Department and Materials Research Institute, Indiana University, Bloomington, Indiana 47405
(Received 13 March 1991)

We calculate the surface power absorption for various models of the electromagnetic fields near jellium metal surfaces, using both the d-parameter formalism and Fermi's golden rule. With Na as a test case, the absorption from an incident electromagnetic wave is examined over the frequency range between zero and twice the plasma frequency. The nature of the surface power absorption is clarified by separating it into contributions in which the excited electrons are either photoexcited into vacuum or backscattered into the bulk. We find that the total surface power absorption is well represented by the sum of these two processes, except where the bulk plasmon exists as an undamped excitation. We also show the relationship between our microscopic theory and earlier phenomenological approaches.

I. INTRODUCTION

The d-parameter theory of nonlocal corrections to Fresnel optics has undergone considerable development over the past decade. Following the pioneering calculations of Feibelman for jellium metals,[1] which provided impressive agreement with the photoemisson data from Al of Levinson and Plummer,[2,3] there have been continued refinements and extensions of the computational procedures,[4] as well as additional confirmations of their experimental relevance.[5–7] In this paper we explore several implications of the theory that further illustrate its physical content. The emphasis is on the evaluation and interpretation of the imaginary part of the d parameter.

For a jellium model of a metal the algebraically simplest way to express the d parameter is as the center of mass (measured, say, from the jellium edge) of the screening charge distribution:

$$d = \int dx\, x\delta\rho \Big/ \int dx\, \delta\rho \ . \tag{1}$$

Here x is the coordinate along the surface normal and the uniform positive background of the jellium lies in $x>0$. The distribution $\delta\rho=\delta\rho(x,\omega)$ represents the linearly induced, nonretarded, screening response of the electrons to a uniform field applied along the surface normal at frequency ω. The real part of d can be thought of as an effective location of the surface, but the interpretation of the imaginary part of d, $\mathrm{Im}(d)$, is less obvious although one knows that it is related to dissipation.[1] We aim to develop this connection more fully by both algebraic manipulations and model calculations. To simplify the analysis we limit ourselves to jellium models, where only surface effects can provide a mechanism for light absorption. Then the computations, once one introduces a mean-field treatment of the many-body interactions, can be done with no further approximation.

We explicitly show how $\mathrm{Im}(d)$ can (usually) be calculated from the efficiency of photoexcitation of electrons into various final-state channels. The basic idea is to reexpress $\mathrm{Im}(d)$, which describes the total optical absorption in jellium models, in terms of a sum of golden-rule transition rates, where the forms of the final electronic states are chosen to represent the various excitation channels. Then one can quantify as a function of photon energy how much of $\mathrm{Im}(d)$ is determined by the excitation of photoemitted electrons and how much by the excitation of electrons that propagate into the bulk. The relative size of these contributions is a sensitive function of both ω and the shape of the surface barrier that holds the bound electrons in the metal. Surface photoabsorption can also excite bulk plasmons over a limited range of ω. Although this contribution is included in $\mathrm{Im}(d)$, we have not found a way to express it in a golden-rule form.

As we will acknowledge in detail later, there have been many previous estimates of the spectral strength of photoexcitation efficiencies. In particular the work of Endriz[8] and that of Persson and collaborators[9–12] have served as guides to the present approach. However, Endriz used a hydrodynamic approximation for the excitation fields while Persson and collaborators only examined low frequencies where the static form of the excitation fields suffices. Our detailed analysis improves on their work primarily by incorporating a better description of the electromagnetic fields near a jellium metal surface, both below and above the bulk-plasmon energy.

In Sec. II we present the equations that define our model and the quantities it can determine. Much of the algebra is relegated to an appendix. Then in Sec. III we show the results of our model calculations and discuss their implications, applications, and limitations. Finally in Sec. IV we briefly relate our approach to some alternate formulations.

II. BASIC EQUATIONS

We begin by expressing the average rate of Joule heating in several ways. First we define it when a monochromatic field is present as

$$\Gamma(\omega)=\frac{1}{2A}\mathrm{Re}\left[\int d^3x\, \mathbf{J}\cdot\mathbf{E}^*\right] , \tag{2}$$

where A is the surface area, Re denotes "real part of," and $\mathbf{J}$ and $\mathbf{E}$ are the complex vector amplitudes of the

current density and total electric field, respectively. In the Appendix we show, for a jellium model with no bulk dissipation subjected to an incident p wave at angle θ, that[1]

$$\Gamma=\frac{\omega}{8\pi}(1-\epsilon)\epsilon|\mathbf{E}_{\rm inc}|^2|t|^2\sin^2\theta\,{\rm Im}(d)\ , \tag{3}$$

where $\mathbf{E}_{\rm inc}$ is the incident field amplitude and t is a Fresnel transmission amplitude,

$$t=\frac{2\cos\theta}{\epsilon\cos\theta+\sqrt{\epsilon-\sin^2\theta}}\ , \tag{4}$$

with

$$\epsilon=1-\omega_p^2/\omega^2\ , \tag{5}$$

the bulk dielectric function of an electron gas with plasma frequency ω_p. In Eq. (3) only ${\rm Im}(d)$ depends on the microscopic details of the surface.

We also show in the Appendix how one may (usually) transform Γ into

$$\Gamma=\hbar\omega\frac{1/\tau}{A}\ , \tag{6}$$

where $1/\tau$ is a golden-rule transition rate. For a jellium model with a flat surface, $1/\tau$ can be considerably simplified since only the normal component of the field can cause transitions:

$$\frac{1/\tau}{A}=\left[\frac{2\pi}{\hbar}\int\frac{d^2K}{(2\pi)^2}\int_0^\infty\frac{dk}{2\pi}\int_0^\infty\frac{dk'}{2\pi}n_{\mathbf{k}}(1-n_{\mathbf{k}'})|M|\delta(\varepsilon_{\mathbf{k}}+\hbar\omega-\varepsilon_{\mathbf{k}'})\right]\left[\frac{e\hbar}{2mc}\right]^2\left|\frac{c}{\omega}\mathbf{E}_{\rm inc}\right|^2|t|^2\sin^2\theta\ , \tag{7}$$

where $\mathbf{K}$ is the (conserved) electron wave vector parallel to the surface while $\mathbf{k},\mathbf{k}'$ are wave vectors for motion normal to the surface, and the $n_{\mathbf{k}}$ are occupation factors requiring at zero temperature that the eigenenergy $\varepsilon_{\mathbf{k}}$ be below the Fermi energy ε_F. The (one-dimensional) matrix element M is

$$M=\left\langle\varphi_{k'}\left|\frac{1}{2}\left[\frac{d}{dx}a+a\frac{d}{dx}\right]\right|\varphi_k\right\rangle\ , \tag{8}$$

where the $|\varphi_k\rangle$ are eigenstates of motion along x, normalized to 2π times a δ function on k and $a(x)$ is a scaled form of $E_x(x)$ given by

$$a(x)=\epsilon+(1-\epsilon)\eta(x)\ , \tag{9}$$

where the dimensionless, but complex-valued $\eta(x)$ starts from zero far out in the vacuum and ends at one deep in the bulk.

Finally we can express Γ in terms of a photoexcitation yield Y if we introduce the incident flux of photons

$$F=\frac{c}{8\pi}|\mathbf{E}_{\rm inc}|^2\cos\theta/\hbar\omega\ . \tag{10}$$

Then

$$\Gamma=\hbar\omega FY\ . \tag{11}$$

The specification of excitation channels for Y is made when one chooses the final states contributing to Eq. (7), since

$$Y=\frac{1/\tau}{A}\Big/F\ . \tag{12}$$

We have carried through a series of evaluations of Eq. (7), based on different models of the surface barrier. In each case we use for the spatial variation of $E_x(x)$ results from the codes of Kempa and Schaich;[4,13–16] i.e., $\eta(x)$ in Eq. (9) is calculated using the same surface barrier. This consistency is a necessary (but not sufficient) condition for the equivalence of the various expressions of Γ. The lack of such consistency is a serious limitation in Endriz's calculations.[8]

The first model system we consider uses an infinite barrier to confine the electrons in the metal. All the orbitals then have the same form

$$\varphi_k(x)=2\sin(kx),\quad 0<x\ , \tag{13}$$

where the origin for x is now at the infinite barrier. We put the energy zero at the bottom of the bulk band, so the eigenenergy is simply

$$\varepsilon_{\mathbf{k}}=\varepsilon_k+\varepsilon_{\mathbf{K}}=\frac{\hbar^2}{2m}(k^2+K^2)\ , \tag{14}$$

where we distinguish the energy of normal motion, ε_k, from the total energy $\varepsilon_{\mathbf{k}}$. The form of (13) is sufficiently simple that a considerable part of the analysis can be done analytically,[13,14,17] but the model allows no photoemission at all.

Our second model system uses a finite, single-step barrier to remove this constraint. Electron states bound in the metal appear as

$$\varphi_k(x)=\begin{cases}2\sin(kx+\delta) & 0<x\ ,\\ \beta e^{px} & x<0\ ,\end{cases} \tag{15}$$

where $x=0$ is at the step and $(\hbar^2/2m)(p^2+k^2)=V_0$ is the step height of the potential-energy barrier and equals the sum of the Fermi energy and the work function. The phase shift $\delta=\tan^{-1}(k/p)$ and amplitude $\beta=2\sin\delta$ are easily found from matching the value and derivative of φ_k across $x=0$. All the initial states have the form (15), and so do the final states whose normal energy is below V_0.

When $\hbar\omega$ exceeds the photoemission threshold, $V_0-\epsilon_F$, a new excitation channel opens and one must consider separately transitions into two orthogonal but degenerate states. We write these two states as

$$\varphi_f(x)=\begin{cases}te^{-igx} & 0<x\\ e^{-ifx}+re^{ifx} & x<0\end{cases} \tag{16}$$

and

$$\tilde{\varphi}_g(x)=\begin{cases} e^{+igx}+\tilde{r}e^{-igx} & 0<x \\ \tilde{t}e^{+ifx} & x<0\ , \end{cases} \tag{17}$$

where

$$V_0<\frac{\hbar^2 g^2}{2m}=\frac{\hbar^2 f^2}{2m}+V_0 \tag{18}$$

and again the matching coefficients are easily determined. We have changed in Eqs. (16) and (17) the wave-vector label from k' to either g or f, which are the wave vectors for free motion either inside or outside the metal. The φ_f are the appropriate final states for photoemission and are normalized to $\langle\varphi_f|\varphi_{f'}\rangle=2\pi\delta(f-f')$,[18] while the $\tilde{\varphi}_g$ represent electrons that propagate into the bulk and are normalized to $\langle\tilde{\varphi}_{g'}|\tilde{\varphi}_g\rangle=2\pi\delta(g-g')$. Transitions into the $\tilde{\varphi}_g$ of Eq. (17) or the φ_k of Eq. (15) are called backscattering events.[8]

The two models described so far have simple barrier shapes that allow analytic solutions to Schrödinger's equation. However, a more fundamental approach would specify the form of the positive background charge alone and then calculate (rather than prescribe) the surface potential-energy barrier. Our third model follows this approach by using the potential-energy barrier self-consistently calculated by Lang and Kohn[19] in a scheme that includes a local-density-functional allowance (LDA) for the influence of exchange and correlation on the single-particle orbitals. The barrier shape is only known numerically, and likewise the eigenstates. However, the asymptotic forms of the ϕ_k's are the same as in Eqs. (15)–(17) so the normalizations and orthogonality, which are set by the long-range behavior, are the same as they are there. One must numerically integrate Schrödinger's equation through the surface region (where the potential-energy function varies with x) in order to find the matching coefficients.

Having described the electron states, let us reexpress the yield into particular channels by substituting Eq. (7) and Eq. (10) into Eq. (12). For photoemission we obtain

$$Y_{\rm PE}=\frac{\alpha}{\pi}\left[\frac{|t|^2\sin^2\theta}{\cos\theta}\right]\int\frac{dk}{f}\int\frac{d\epsilon_K}{\hbar\omega}|M_{fk}|^2$$
$$\times\Theta(\epsilon_F-\epsilon_{\rm k})\Theta(\epsilon_{\rm k}+\hbar\omega-\epsilon_F)\Theta(\epsilon_k+\hbar\omega-V_0)\ , \tag{19}$$

where $\alpha=e^2/\hbar c$, and the three Θ functions ensure that the initial state is occupied and that the final state is above ϵ_F and possesses sufficient normal energy to propagate in the vacuum. The backscattering yield $Y_{\rm BS}$ has the same general form except for modifications of the last Θ-function argument and the replacement of f with g or k', depending on whether the final normal energy is above or below the vacuum level, respectively. In all cases the integral over the parallel energy ϵ_K can be done analytically since K does not enter the matrix element. Note, too, that the dependence on the photon angle of incidence comes only from the simple factors in the large parentheses.[8,20]

As a final technical point before turning to results, we remark that we will consider the effect of two different η functions in Eq. (9) for the Lang-Kohn barrier model. The first is calculated, as for the infinite barrier and single-step models, within the random-phase approximation (RPA), while the second is more consistently determined by using a time-dependent LDA. The latter procedure treats the optical response on the same basis as the ground state. Not only does this produce different values for $\eta(x)$, but also there is an additional contribution to the matrix element (8). Its derivation is given in the Appendix.

III. RESULTS

In all our model calculations we choose parameters for the jellium so it mimics Na. For the infinite barrier model the description of the bulk density by $r_s=3.99$ fixes the only free parameter aside from the frequency, which we measure by ratio to the bulk plasma frequency ω_p. Figure 1 plots various estimates of $\mathrm{Im}(d)$ for this model calculated from the (presumed) equivalence of Eqs. (3) and (6). Note from Eqs. (3) and (5) that $\mathrm{Im}(d)<0$ when $\epsilon<0$; i.e., when $\omega<\omega_p$.

In the simplest calculation we ignore the spatial variation of the field and set a to one. Then the matrix element M in Eq. (8) using the eigenstates of Eq. (13) is simply $M=2\hbar k'k/m\omega$. The resulting $\mathrm{Im}(d)$ diverges at ω_p and is everywhere much too strong. Next we use a non-self-consistent but spatially varying estimate of a as provided by the single-step hydrodynamic model.[21] One writes $\eta(x>0)$ as

$$\eta(x>0)\approx 1-e^{ipx}\ , \tag{20}$$

where

$$p^2=\frac{\omega^2-\omega_p^2}{\beta^2}\ , \tag{21}$$

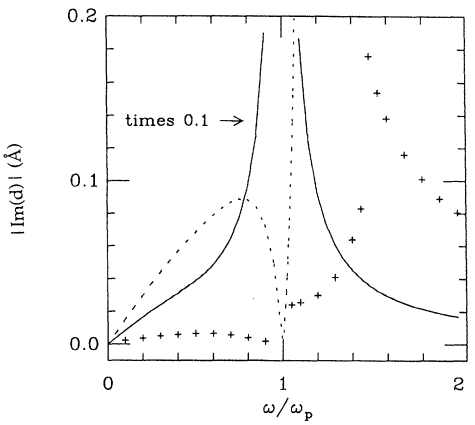

FIG. 1. Absolute value of the golden-rule estimate of $\mathrm{Im}(d)$ for the infinite barrier model vs photon frequency ω. For the solid curve, the scaled field $a=1$ and the results have been reduced by a factor of 10 to fit in the graph. For the dashed curve the single-step hydrodynamic field is used for a. The points come from an evaluation based on the RPA a. For all cases only backscattering events contribute.

with $\beta^2=\frac{3}{5}v_F^2$ and v_F the Fermi velocity. The η function is slowly varying when ω is near ω_p, which dramatically suppresses the absorption. However, the inconsistency of this calculation becomes apparent above ω_p where its predictions diverge when the plasmon dispersion implicit in Eq. (21) enters the particle-hole continuum for $\omega/\omega_p \approx 1.2$. This deficiency occurs in Endriz's calculations, too,[8] and is only removed by allowing the absorption to self-consistently damp out the plasmons.

The results for such a calculation, using the RPA η, are also shown in Fig. 1. There are three regions of distinct behavior. Below ω_p, Im(d) is very small and has no sharp structure. For $\omega_p < \omega < \omega_{\rm LD}$ where $\omega_{\rm LD} \approx 1.48\omega_p$ is the onset of Landau damping for the RPA plasmon,[16] Im(d) is larger and growing as $\omega \to \omega_{\rm LD}$. Finally for $\omega > \omega_{\rm LD}$, Im(d) smoothly decays. Calculations cannot be reliably done in the near vicinity of the boundary frequencies ω_p and $\omega_{\rm LD}$, so we have not plotted cases where the numerical uncertainty probably exceeds the size of the symbol. It can consequently be difficult to tell if Im(d) diverges at a boundary. Such difficulties become worse for the more sophisticated models to which we now turn.

Figure 2 shows results for the single-step model. We keep $r_s=3.99$ and impose a work function of 2.7 eV$=\hbar\omega_0$, which sets a threshold. Photoemission can only occur above ω_0. The separate contributions of backscattering and photoemission channels are quite different close to ω_p but become nearly equal above $\omega_{\rm LD}$. Note, too, the large increase in absorption strength compared to Fig. 1, at least above threshold.

Finally, in Fig. 3 we present the analogous results for the Lang-Kohn barrier model, using the η from a RPA response calculation. For this case $r_s=4$ and the photoemission threshold is at $\omega_0/\omega_p=0.51$. The absorption strength is somewhat stronger than in Fig. 2 and the two channels contribute with roughly equal strength for most frequencies above threshold.

The striking new feature is the appearance of a resonance in each contribution to Im(d) for $0.8 < \omega/\omega_p < 0.9$. Similar structure occurs in this relative frequency range for all metallic r_s values.[22] The corresponding peak in the photoemission yield for Al was the first major success of the theory[1-3] and the same behavior has been reported for several additional systems.[23,24] It also seems to be apparent in earlier data by Monin and Boutry for the alkali metals,[25] but the particular case of Na is puzzling since the experimental peak occurs at $\omega/\omega_p=0.66$ and the data do not go beyond $\omega/\omega_p=0.8$. We urge that one remeasure Na over a wider frequency range to see if there is a peak above $0.8\omega_p$ or if the reported one is due to surface-plasmon coupling. The maximum yield per incident electron that we calculate (for both RPA and LDA) is less than a factor of 2 larger than that in the data of Ref. 25.

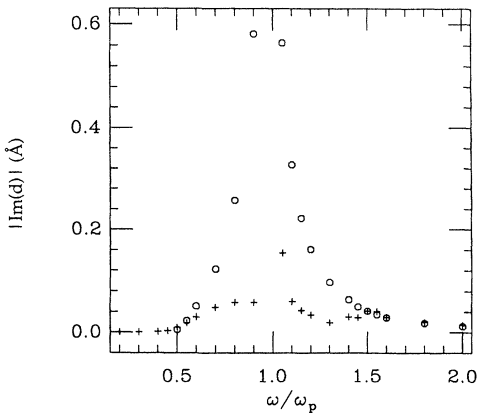

FIG. 2. Absolute value of the golden-rule contributions to Im(d) for the single-step barrier model vs photon frequency ω. The +'s and ○'s are the separate contributions of the backscattering and photoemission excitation channels, respectively. The latter vanish below the threshold at $\omega_0/\omega_p=0.46$.

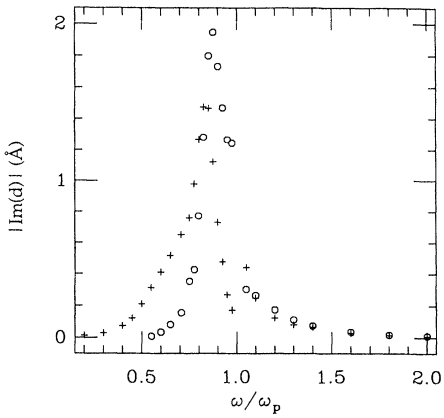

FIG. 3. Absolute value of the golden-rule contributions to Im(d) for the Lang-Kohn barrier model vs photon frequency. The plotted symbols have the same meaning as in Fig. 2.

Up to this point we have determined contributions to Im(d) by combining Eqs. (3) and (6). Now consider whether these results are consistent with the predictions of Eq. (1), which is the standard route to d. In Figs. 4–6 we plot both the sum of the golden-rule results and the alternate predictions from Eq. (1). The comparison is clearest in Fig. 4: the two theoretical approaches agree well except when $\omega_p < \omega < \omega_{\rm LD}$; i.e., except when the bulk plasmon can freely propagate. Before describing the reasons for this situation, we discuss the validity of the same inference from Figs. 5 and 6.

The problem with these more involved calculations is their larger intrinsic errors. Our codes for finding η become less accurate not only for ω close to ω_p or $\omega_{\rm LD}$, but also for $\omega \ll \omega_p$ or $\omega \gg \omega_p$ since in both limits d is small. We have purposely chosen the size of the symbols plotted in Figs. 5 and 6 to represent roughly the numerical uncertainty of our results. Hence, at any frequency where the symbols partially overlap, one may infer equivalence. Within these limitations, it is again only the region $\omega_p < \omega < \omega_{\rm LD}$ where the two estimates significantly differ.[26]

Although there are no alternate evaluations to compare with at the highest frequencies, we remark that many have examined the low-frequency limit, where it is

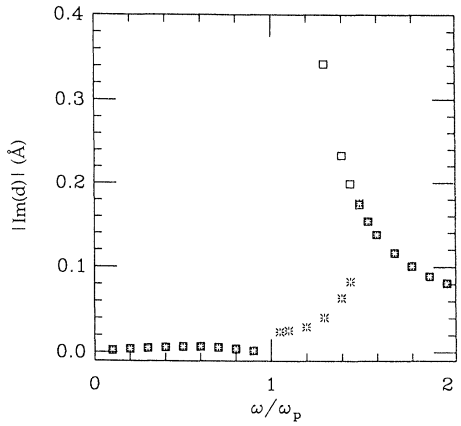

FIG. 4. Absolute value of Im(d) for the infinite barrier model vs photon frequency ω. The bursts are found from a golden-rule calculation, and the squares are obtained from the dipole moment of the induced screening charge. Both calculations are done with the same η function.

well known that Im(d) vanishes linearly with ω. Indeed it is just in this limit that Persson and collaborators introduced the presumed validity of the golden-rule approach to Im(d).[9–12] A motivation for their work was to estimate the nonradiative rate of decay of an oscillating dipole near the metal surface.[27–30] For comparison with experiment, Im(d) is not the sole relevant quantity since it only describes the long-range effect of the surface.[31] A complete theory of the decay must also include a Fresnel term that arises from dissipation in the bulk and accounts for short-range couplings.[32–36] There are also arguments that when the oscillating dipole is replaced by a realistic absorbate, one must include charge-transfer processes with the substrate, as well as electrodynamic coupling.[37–40] But to return to our question of the equivalence of different approaches to Im(d), we note that in the low-frequency limit it has been explicitly checked and confirmed only by Liebsch.[22] This paper gives both the LDA and RPA cases and references the earlier, unsuccessful, checks. For the confirmation to succeed one must include "surface, bulk, and interference" terms in the golden-rule estimate[12,22,41] (i.e., evaluate M with no approximations), as well as allow for exchange-correlation couplings in the LDA,[22,41] as described in the Appendix.

Let us now come back to consider the regime of plasmon propagation where the golden-rule calculations significantly underestimate Im(d). A mathematical reason for this failure is evident in the "proof" of (6) outlined in the Appendix, specifically at the point where one integrates by parts in Eq. (A11) and assumes that the induced longitudinal fields have decayed to zero far from the surface. A propagating plasmon by definition does not decay, so the formal proof fails as confirmed by the numerical results in Figs. 4–6.

We tried to patch up the relation (6) to include a plasmon contribution. Consider a hydrodynamical model, which retains only the plasmon degree of freedom. With a single density step, one has, using (20) and (21)

$$d=\int_0^\infty dx\,[1-\eta(x)]=i/p\ , \tag{22}$$

so above ω_p, $\mathrm{Im}(d)=\beta/\sqrt{\omega^2-\omega_p^2}$. This estimate qualitatively agrees with the deficiency of the golden-rule re-

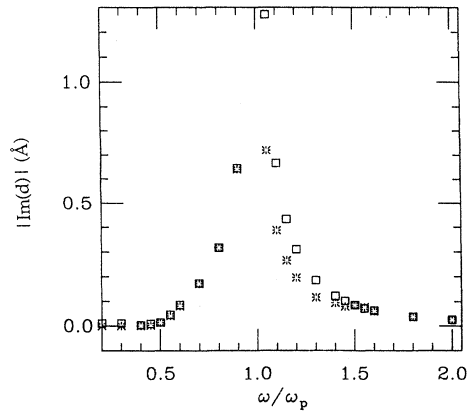

FIG. 5. Same as Fig. 4 except that the model is the single-step barrier.

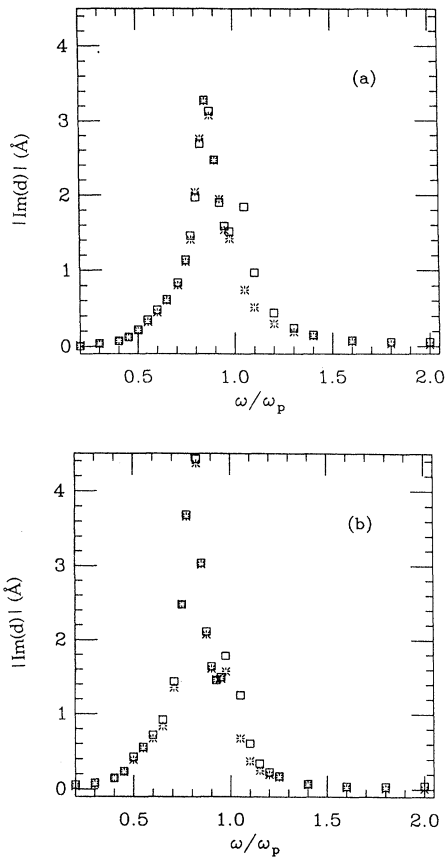

FIG. 6. Same as Fig. 4 except that the model is the Lang-Kohn barrier. In (a) a RPA calculation of η and Im(d) is done and Landau damping begins (as in Figs. 1–5) above $\omega_{\mathrm{LD}}=1.48\omega_p$. In (b) a LDA calculation of η and Im(d) is done and Landau damping begins above $\omega_{\mathrm{LD}}=1.32\omega_p$.

sults, especially if one scales it with the probability of exciting a bulk plasmon in the more realistic models.[16] However we never could match quantitatively to the Im(d) from (1); i.e., we cannot meaningfully express Im(d) for $\omega_p < \omega < \omega_{LD}$ as the sum of single-particle and collective mode absorption.

IV. ALTERNATE THEORIES

In this last section we compare several different approaches with ours. We begin with phenomenological theories of photoemission yield which aim to express Y_{PE} in terms of fields and currents alone, avoiding electron eigenstates and matrix elements. The physical idea is to associate Y_{PE} with a fraction of the total power absorption that occurs near the surface. For instance Kliewer's result[42,43] is in our notation

$$Y_{PE} = \frac{\Gamma_K}{\hbar\omega F} , \tag{23}$$

where

$$\Gamma_K = \frac{1}{2A}\mathrm{Re}\left[\int_{x>0} d^3x\, \mathbf{J}\cdot\mathbf{E}^* e^{-x/\lambda}\right] . \tag{24}$$

Note the appearance of an exponential cutoff in the integrand with the sampling depth λ. Given λ, the evaluation of (23) and (24) only requires $\mathbf{J}$ and $\mathbf{E}$, for which Kliewer invokes the semiclassical infinite behavior approximation which uses bulk properties alone to determine the surface behavior. We do not directly compare his numerical results with ours except to note that the three surface barrier models treated here have quite different answers, while Kliewer's theory would predict a single spectrum once the bulk r_s is set.

Forstmann and collaborators[44,45] have argued that $\mathbf{J}\cdot\mathbf{E}^*$ is not an appropriate measure of local absorption density and suggest that the Γ_K in (24) should be replaced by

$$\Gamma_F = \frac{1}{2A}\mathrm{Re}\left[\int_{x>0} d^3x \frac{4\pi\gamma}{\omega_p^2}|\mathbf{J}|^2 e^{-x/\lambda}\right] , \tag{25}$$

where the new damping parameter γ is assumed to be constant. To evaluate their theory they use hydrodynamic models of the surface response, which introduces further parameters like β of (21) and $\omega_p(x)$. For a two-step equilibrium density model they can reproduce the resonance peak near $\omega/\omega_p \approx 0.8$. However, the success is more that of fitting known results than predicting new ones. There is no way to calculate *a priori* the several required parameters. The theory also shares with Kliewer's the flaw of predicting nonzero photoemission yield below threshold. Within these limitations, the theory does have the virtue of simplicity and gives one insights into some of the physics. We have examined how the predictions of these theories change when the numerically exact fields for a particular barrier model are used. There is some improvement but the basic limitations remain.

Finally we consider the theory of surface-plasmon-assisted optical absorption proposed by Sievers[46,47] to account for anomalies in the optical properties of the alkali metals. Without repeating the rationale and derivation behind his work, let us jump to the implications of his results, which can be compared to those found here. Both his model and ours assume the basic system is jellium with neither band structure nor dissipation in the bulk. Hence the predicted optical properties should be the same, which means that the reflection amplitudes of light should agree, which means that d parameters should be the same. We'll see, however, that the predicted d's are quite different.

This demonstration requires some preliminary algebra because Sievers did not present his results as d parameters. Instead he described them by saying that the system behaved optically as if it has no surface corrections but, instead, a bulk dielectric function of

$$\tilde{\epsilon}(\omega) = 1 - \frac{\omega_p^2 m/m^*}{\omega^2 + i\omega/\tau} \tag{26}$$

to replace the $\epsilon(\omega)$ of (5). Treating his correction parameters, $\lambda(\omega) = m^*(\omega)/m - 1$ and $[\omega\tau(\omega)]^{-1}$ as small compared to unity one can easily expand the difference $\Delta\epsilon$,

$$\Delta\epsilon = \tilde{\epsilon} - \epsilon \approx (1-\epsilon)(\lambda + i/\omega\tau) . \tag{27}$$

This (presumed) slight difference of bulk dielectric functions in (27) produces a small difference in reflection and transmission amplitudes, which can be described by so-called pseudo-d-parameters defined via[48]

$$\tilde{d} = \frac{ic}{2\omega}\frac{\Delta\epsilon}{\epsilon}\Big/(\epsilon - \sin^2\theta)^{1/2} . \tag{28}$$

Combining (27) and (28) we obtain for $\omega < \omega_p$,

$$|\mathrm{Im}(\tilde{d})| = \frac{c}{2\omega}\frac{\omega_p^2/\omega^2}{|\epsilon|\omega\tau(\omega_p^2/\omega^2 - \cos^2\theta)^{1/2}} > \frac{c}{2\omega_p}\left[\frac{1}{\omega\tau}\right] . \tag{29}$$

But for Na, $c/c\omega_p = 167$ Å and from Fig. 5 in Ref. 47, $(\omega\tau)^{-1}$ is always larger than 0.03 for $1 < \hbar\omega < 3$ eV. Hence Sievers's model predicts that $|\mathrm{Im}(\tilde{d})| > 5$ Å over this range, which corresponds to $0.17 < \omega/\omega_p < 0.51$. Looking at Figs. 4–6 here one sees that our values of $|\mathrm{Im}(d)|$ are at least an order of magnitude smaller than 5 Å in this frequency range.

We believe that our calculations correctly describe the jellium response[4] and assert that Sievers has greatly overestimated the effect of surface-plasmon-assisted absorption. In fact the overall coupling strength is a free parameter in his model, which he chose by comparison with experimental data. We feel that this is an incorrect procedure. The difference between experiment and our jellium model predictions is not a serious concern until one incorporates crystallinity effects into the calculation of the bulk ϵ and the surface d's. We have begun such an effort.[49]

ACKNOWLEDGMENTS

We thank Dr. N. D. Lang for sending us the numerical output describing his surface barriers. Our work was

supported in part by the National Science Foundation through Grant No. DMR-89-03851. Some of the calculations were done on the Cray Research, Inc., Y-MP4/464 system at the National Center for Supercomputing Applications at the University of Illinois at Urbana-Champaign (Champaign, IL).

APPENDIX

We derive several formal relations between different approaches to Im(d). Begin with the path between Eqs. (2) and (3). For a long-wavelength photon field incident on jellium, the key integral in (2) is along the surface normal:

$$\Gamma=\tfrac{1}{2}\mathrm{Re}\left[\int dx\ \mathbf{J}\cdot\mathbf{E}^*\right] . \tag{A1}$$

Replacing $\mathbf{J}$ with the difference between the microscopic $\mathbf{E}$ and $\mathbf{D}$ fields,

$$\mathbf{J}=i\frac{\omega}{4\pi}(\mathbf{E}-\mathbf{D}) , \tag{A2}$$

yields

$$\Gamma=\frac{\omega}{4\pi}\mathrm{Im}\left[\int dx\ \mathbf{D}\cdot\mathbf{E}^*\right] . \tag{A3}$$

The response at the flat jellium surface to an optical field[1,50] allows one to write

$$\Gamma=\frac{\omega}{4\pi}\mathrm{Im}\left[\int dx(D_\perp E_\perp^*+D_\parallel E_\parallel^*)\right] , \tag{A4}$$

where the field components $D_\perp$ and $E_\parallel$ are nearly constant over the surface region. If we view the other field components as determined by a nonlocal, microscopic, diagonal (in the long-wavelength limit) dielectric tensor, then[50]

$$\Gamma=\frac{\omega}{4\pi}\mathrm{Im}\left[|D_\perp|^2\int dx(\epsilon^{-1})^*_{\perp,\perp}+|E_\parallel|^2\int dx\ \epsilon_{\parallel,\parallel}\right] . \tag{A5}$$

Finally we recall the formal definition of the d parameters[1,50]

$$(1-\epsilon)\mathrm{Im}(d_\parallel)=\mathrm{Im}\left[\int dx\ \epsilon_{\parallel,\parallel}\right] , \tag{A6}$$

$$(1-1/\epsilon)\mathrm{Im}(d_\perp)=\mathrm{Im}\left[\int dx(\epsilon^{-1})_{ppd,\perp}\right] , \tag{A7}$$

where ϵ is given by Eq. (5). Substituting these in (A5) yields

$$\Gamma=\frac{\omega}{8\pi}(1-\epsilon)\left[\frac{|D_\perp|^2}{\epsilon}\mathrm{Im}(d_\perp)+|E_\parallel|^2\mathrm{Im}(d_\parallel)\right] . \tag{A8}$$

Actually, for jellium, $d_\parallel$ is a real valued constant, so in the text we have simply used d for $d_\perp$. Finally, to get (3) we note that by Fresnel optics

$$D_\perp=\epsilon t E_{\mathrm{inc}}\sin\theta . \tag{A9}$$

Next we outline the route from Eqs. (2) to (6). It is sufficient to calculate (2) using electrostatic fields so we may write

$$\mathbf{E}=-\nabla\Phi \tag{A10}$$

and integrate by parts in (2)

$$\Gamma=\frac{1}{2A}\mathrm{Re}\left[\int d^3x\ \mathbf{J}\cdot(-\nabla\Phi)^*\right]$$
$$=\frac{1}{2A}\mathrm{Re}\left[\int d^3x\ \Phi^*(\nabla\cdot\mathbf{J})\right] , \tag{A11}$$

neglecting any contributions from the limits of the integrals. As discussed in the text, the transformation in (A11) is not always justified. Let us proceed anyway, replacing $\nabla\cdot\mathbf{J}$ via the equation of continuity with $i\omega e\delta\rho$, where $e\delta\rho$ is the induced charge density. Then

$$\Gamma=-\frac{\omega e}{2A}\mathrm{Im}\left[\int d^3x\ \Phi^*(\mathbf{x})\delta\rho(\mathbf{x})\right] . \tag{A12}$$

In our mean-field treatment of many-body effects, $\delta\rho$ is determined by the independent-particle susceptibility as

$$\delta\rho(\mathbf{x})=\int d^3x'\chi_0(\mathbf{x},\mathbf{x}';\omega)e\Phi(\mathbf{x}') , \tag{A13}$$

where

$$\chi_0(\mathbf{x},\mathbf{x}';\omega)=\sum_{\alpha,\beta}\frac{n_\alpha-n_\beta}{\epsilon_\alpha+\hbar\omega-\epsilon_\beta+i0^+}$$
$$\times\Psi^*_\alpha(\mathbf{x})\Psi_\beta(\mathbf{x})\Psi^*_\beta(\mathbf{x}')\Psi_\alpha(\mathbf{x}') . \tag{A14}$$

The sums run over the labels of single-particle eigenstates and the n_α are occupation factors. Combining (A12)–(A14) we obtain

$$\Gamma=\frac{\pi\omega}{2A}\sum_{\alpha,\beta}(n_\alpha-n_\beta)|\langle\beta|e\Phi|\alpha\rangle|^2\delta(\epsilon_\alpha+\hbar\omega-\epsilon_\beta) . \tag{A15}$$

The energy-conserving δ function allows us at zero temperature to replace the factor $n_\alpha-n_\beta$ with $n_\alpha(1-n_\beta)$ so

$$\Gamma=\frac{\hbar\omega}{A}\left[\frac{2\pi}{\hbar}\sum_{\alpha,\beta}n_\alpha(1-n_\beta)\left|\left\langle\beta\left|\frac{e}{2}\Phi\right|\alpha\right\rangle\right|^2\right.$$
$$\left.\times\delta(\epsilon_\alpha+\hbar\omega-\epsilon_\beta)\right] , \tag{A16}$$

which is (6). The factor of $\frac{1}{2}$ in the matrix element appears because Φ is a complex amplitude. The real valued scalar potential is $\frac{1}{2}(\Phi e^{-i\omega t}+\Phi^* e^{i\omega t})$ and only the first term leads to energy absorption for $\omega>0$.

We do not calculate matrix elements of Φ but instead change to matrix elements of a vector potential by using a standard commutator trick:

$$\langle\beta|e\Phi|\alpha\rangle=\langle\beta|[H,e\Phi]|\alpha\rangle/\hbar\omega$$
$$=\frac{-ie}{2m\omega}\langle\beta|(\mathbf{p}\cdot\nabla\Phi+\nabla\Phi\cdot\mathbf{p})|\alpha\rangle$$
$$=\frac{ie}{2m\omega}\langle\beta|(\mathbf{p}\cdot\mathbf{E}+\mathbf{E}\cdot\mathbf{p})|\alpha\rangle$$
$$=\frac{-e}{2mc}\langle\beta|(\mathbf{p}\cdot\mathbf{A}+\mathbf{A}\cdot\mathbf{p})|\alpha\rangle , \tag{A17}$$

where $-\nabla\Phi=\mathbf{E}=(i\omega/c)\mathbf{A}$ and $\mathbf{p}=(\hbar/i)\nabla$. Equation

(A17) easily scales into the M of (8).

The derivation in the above paragraph is unambiguous for a RPA calculation of the response. For that case Φ is simply the Hartree potential. But for a LDA calculation one must augment $e\Phi$ with[15,22,41]

$$\delta\mu_{xc}(x)=V_{xc}(x)\delta\rho(x)\ , \tag{A18}$$

where

$$V_{xc}=\left.\frac{d^2[n\epsilon_{xc}(n)]}{dn^2}\right|_{n=n_0(x)}\ , \tag{A19}$$

with ϵ_{xc} the exchange-correlation energy per electron in a uniform electron gas of density n and $n_0(x)$ the equilibrium density of electrons at x. We use the V_{xc} of Hedin and Lundqvist[51] and employ (A17) to transform (A18) into an additional contribution to **A**.

[1]P. J. Feibelman, Prog. Surf. Sci. **12**, 287 (1982).
[2]H. J. Levinson, E. W. Plummer, and P. J. Feibelman, Phys. Rev. Lett. **43**, 952 (1979).
[3]H. J. Levinson and E. W. Plummer, Phys. Rev. B **24**, 628 (1981).
[4]K. Kempa, A. Liebsch, and W. L. Schaich, Phys. Rev. B **38**, 12 645 (1988).
[5]K.-D. Tsuei, E. W. Plummer, and P. J. Feibelman, Phys. Rev. Lett. **63**, 2256 (1989).
[6]K.-D. Tsuei, E. W. Plummer, A. Liebsch, K. Kempa, and P. Bakshi, Phys. Rev. Lett. **64**, 44 (1990).
[7]A. Liebsch, G. Hincelin, and T. López-Rios, Phys. Rev. B **41**, 10 463 (1990).
[8]J. G. Endriz, Phys. Rev. B **7**, 3464 (1973).
[9]B. N. J. Persson and N. D. Lang, Phys. Rev. B **26**, 5409 (1982).
[10]B. N. J. Persson, Phys. Rev. Lett. **50**, 1089 (1983).
[11]B. N. J. Persson, Phys. Rev. B **29**, 4382 (1984).
[12]B. N. J. Persson and E. Zaremba, Phys. Rev. B **31**, 1863 (1985).
[13]K. Kempa and W. L. Schaich, Phys. Rev. B **32**, 8375 (1985).
[14]K. Kempa and W. L. Schaich, Phys. Rev. B **34**, 547 (1986).
[15]K. Kempa and W. L. Schaich, Phys. Rev. B **37**, 6187 (1988).
[16]K. Kempa and W. L. Schaich, Phys. Rev. B **39**, 13 139 (1989).
[17]R. R. Gerhardts and K. Kempa, Phys. Rev. B **30**, 5704 (1984).
[18]W. L. Schaich, in *Photoemission in Solids,* edited by M. Cardona and L. Ley (Springer, New York, 1978), Vol. 1.
[19]N. D. Lang and W. Kohn, Phys. Rev. B **1**, 4555 (1970).
[20]J.-T. Lee and W. L. Schaich, Phys. Rev. B **38**, 3747 (1988).
[21]W. L. Schaich and K. Kempa, Phys. Scr. **35**, 204 (1987).
[22]A. Leibsch, Phys. Rev. B **36**, 7378 (1987).
[23]G. Jezaquel, Phys. Rev. Lett. **45**, 1963 (1980).
[24]R. A. Bartynski, E. Jensen, T. Gustafsson, and E. W. Plummer, Phys. Rev. B **32**, 1921 (1985).
[25]J. Monin and G. A. Boutry, Phys. Rev. B **9**, 1309 (1974).
[26]The single apparent exception to this claim occurs in Fig. 6 at $\omega/\omega_p=0.975$ and is probably unreliable (Ref. 4).
[27]R. R. Chance, A. Prock, and R. Silbey, Adv. Chem. Phys. **37**, 1 (1978).
[28]B. N. J. Persson, J. Phys. C **11**, 4251 (1978).
[29]A. Liebsch, Phys. Scr. **35**, 354 (1987).
[30]A. G. Eguiluz, Phys. Scr. **36**, 651 (1987).
[31]P. Apell, Phys. Scr. **24**, 795 (1980).
[32]B. N. J. Persson and M. Persson, Surf. Sci. **97**, 609 (1980).
[33]B. N. J. Persson and W. L. Schaich, J. Phys. C **14**, 5583 (1981).
[34]A. G. Eguiluz, Phys. Rev. Lett. **51**, 1907 (1983); Phys. Rev. B **30**, 4366 (1984).
[35]A. Liebsch, Phys. Rev. Lett. **54**, 67 (1985); Phys. Rev. B **32**, 6255 (1985).
[36]J. Dobson and G. H. Harris, J. Phys. C **19**, 3971 (1986).
[37]B. N. J. Persson and M. Persson, Solid State Commun. **36**, 175 (1980).
[38]B. N. J. Persson and R. Rydberg, Phys. Rev. Lett. **48**, 549 (1982).
[39]Ph. Avouris and B. N. J. Persson, J. Chem. Phys. **88**, 837 (1984).
[40]M. Persson and B. Hellsing, Phys. Rev. Lett. **49**, 662 (1982); Phys. Scr. **29**, 360 (1984).
[41]A. Liebsch, J. Phys. C **19**, 5025 (1986).
[42]K. L. Kliewer, Phys. Rev. B **14**, 1412 (1976); **15**, 3759 (1977).
[43]K. L. Kliewer, in *Photoemission and the Electronic Properties of Surfaces,* edited by B. Feuerbacher, B. Fitton, and R. F. Willis (Wiley, New York, 1978).
[44]K. Kempa and F. Forstmann, Surf. Sci. **129**, 516 (1983).
[45]F. Forstmann and R. R. Gerhardts, *Metal Optics Near the Plasma Frequency* (Springer, Berlin, 1986).
[46]A. J. Sievers, Phys. Rev. Lett. **45**, 386 (1980).
[47]A. J. Sievers, Phys. Rev. B **22**, 1600 (1980).
[48]W. L. Schaich, Phys. Rev. B **37**, 6193 (1988).
[49]J. T. Lee and W. L. Schaich, Phys. Rev. B **43**, 4629 (1991).
[50]W. L. Schaich and W. Chen, Phys. Rev. B **39**, 10 714 (1989).
[51]L. Hedin and B. I. Lundqvist, J. Phys. C **4**, 2064 (1971).